Coupling of the skyrmion velocity to its breathing mode in periodically notched nanotracks

Coupling of the skyrmion velocity to its breathing mode in periodically notched nanotracks

To cite this article before publication: Jonathan Leliaert *et al* 2018 *J. Phys. D: Appl. Phys.* in press https://doi.org/10.1088/1361-6463/aae7c1

Coupling of the skyrmion velocity to its breathing mode in periodically notched nanotracks

J. Leliaert[1], P. Gypens[1], M. V. Milošević[2], B. Van Waeyenberge[1], J. Mulkers[1,2]

[1] Department of Solid State Sciences, Ghent University, Ghent, Belgium
[2] Department of Physics, University of Antwerp, Antwerp, Belgium

E-mail: jonathan.leliaert@ugent.be

Abstract. A thorough understanding of the skyrmion motion through nanotracks is a prerequisite to realize the full potential of spintronic applications like the skyrmion racetrack memory. One of the challenges is to place the data, i.e. skyrmions, on discrete fixed positions, e.g. below a read or write head. In the domain-wall racetrack memory, one proposed solution to this problem was patterning the nanotrack with notches. Following this approach, this paper reports on the skyrmion mobility through a nanotrack with periodic notches (constrictions) made using variations in the chiral Dzyaloshinskii-Moriya interaction. We observe that such notches induce a coupling between the mobility and the skyrmion breathing mode, which manifests itself as velocity-dependent oscillations of the skyrmion diameter and plateaus in which the velocity is independent of the driving force. Despite the fact that domain walls are far more rigid objects than skyrmions, we were able to perform an analogous study and, surprisingly, found even larger plateaus of constant velocity. For both systems it is straightforward to tune the velocity at these plateaus by changing the design of the notched nanotrack geometry, e.g. by varying the distance between the notches. Therefore, the notch-induced coupling between the excited modes and the mobility could offer a strategy to stabilize the velocity against unwanted perturbations in racetrack-like applications. In the last part of the paper we focus on the low-current mobility regimes, whose very rich dynamics at nonzero temperatures are very similar to the operating principle of recently developed probabilistic logic devices. This proves that the mobility of nanomagnetic structures through a periodically modulated track is not only interesting from a fundamental point of view, but has a future in many spintronic applications.

1. Introduction

Nanomagnetic structures are considered as data carriers in nanometer sized, low-power spintronic applications. Amongst these applications, logic [1, 2] and memory devices are most promising, and continual research has resulted in steady advances over the last decade. For instance, starting from the original in-plane magnetic-domain-based racetrack memory [3], several generations with marked improvements were developed [4]. These developments range from data representation in domain walls instead of domains, over the shift towards out-of-plane magnetized materials or the use of antiferromagnetically coupled layers to minimize stray fields. One of the most important recent proposals is an implementation in which data is not longer stored in domain walls, but in topologically protected magnetic bubbles with a diameter of only a few nanometer, called skyrmions [5, 6]. These topological structures can be found in magnetic films with a broken inversion symmetry, allowing for a non-zero chiral Dzyaloshinskii-Moriya interaction (DMI) [7, 8, 9]. In very thin ferromagnetic films, this asymmetry can be induced by the coupling of the ferromagnetic layer to a nonmagnetic layer with a strong spin-orbit coupling [10]. This type of DMI, commonly referred to as the interfacially induced DMI, allows the formation of isolated skyrmions [11]. Recently, skyrmion stability at room temperature [12] and even controlled skyrmion motion have been experimentally demonstrated [13], and the technological know-how to reliably read and write single skyrmions [14] was developed.

However, regardless of the racetrack memory implementation, from the simplest domain-wall based design up to the most advanced skyrmion racetrack, it remains crucial that the motion of the magnetic structures representing the data can be accurately controlled for these devices to operate efficiently and reliably. This is not only important for their basic functioning, e.g. to place the data below a read or write head, but also to ascertain that there remains sufficient distance between the different structures to keep them from colliding. Especially in technological applications which operate in the magnetically noisy environment caused by Oersted fields due to surrounding electronics, the device should be robust against small perturbations. Because of this, the first racetrack memory design already included notches to pin the data to fixed locations [3]. As an interesting side effect, these notches allowed the domain wall to reach higher velocities during their motion through the track [15]; an effect attributed to the suppression of the Walker breakdown, similar to the behavior reported in nanotracks with edge roughness [16]. The use of notches to increase the reliability has also been considered for skyrmion racetrack memories [17], where the interplay between the driving current and the pinning potential on the skyrmion shows nontrivial effects that can be exploited in e.g. skyrmion diodes [18], where the depinning threshold depends on the direction in which the skyrmion encounters the notch. Further interesting results were obtained in the study of a skyrmion lattice in which the skyrmions were approximated by rigid objects, and were excited by a combination of both an AC and a DC driving current [19]. There, the skyrmion motion couples to a periodic two-dimensional potential

landscape, resulting in motion against the electron flow, or regimes in which the velocity is almost independent on the strength of the driving force.

It is clear that the motion of skyrmions through periodically modulated potential landscapes displays rich dynamics, and a full understanding of this motion will be of benefit to the realization of skyrmion-based spintronic devices. In this paper, we study the motion of a skyrmion driven through a nanotrack with periodically placed notches, and show that the notches are able to excite internal skyrmion resonances at certain velocities, where the system exhibits robustness against small perturbations in the driving force. In the second part of the paper, the study is extended to the motion of a current-driven domain wall and we show that, despite the fact that domain walls are far more rigid objects than skyrmions, the mobility displays similar behavior. Finally, the effects of nonzero temperatures on the motion at low driving forces are discussed in the context of future probabilistic skyrmion logic applications.

2. Methods

2.1. Micromagnetic simulations

All micromagnetic simulations were performed using the GPU-accelerated software package MuMax3 [20, 21], to numerically solve the Landau-Lifshitz-Gilbert equation [22] extended with two spin-transfer-torque (STT) terms [23]

$$\dot{\mathbf{m}} = \gamma\mu_0\mathbf{H}_{\text{eff}} \times \mathbf{m} + \alpha\mathbf{m} \times \dot{\mathbf{m}} + [b\mathbf{j} \cdot \nabla]\,\mathbf{m} - \beta\mathbf{m} \times [b\mathbf{j} \cdot \nabla]\,\mathbf{m}. \tag{1}$$

Here, $\mathbf{m}$ is the magnetization, normalized to its saturation value M_{sat}, and $\mathbf{H}_{\text{eff}}$ is the effective field comprised of the exchange, magnetostatic, anisotropy and interfacially induced DMI fields, whose strength is determined by the material constants A_{ex}, M_{sat}, K_u and D denoting the exchange constant, the saturation magnetization, the uniaxial anisotropy constant, and the interfacially-induced DMI parameter, respectively. Furthermore, the gyromagnetic ratio, the vacuum permeability and the phenomenological damping constant are given by $\gamma = 28.02495$ GHz/T, $\mu_0 = 4\pi \times 10^{-7}$ Tm/A, and α, for which we used a value of 0.01 in our simulations. In the last two terms, $\mathbf{j}$ denotes the charge current density, β the degree of non-adiabaticity, and

$$b = \frac{P\mu_{\text{B}}}{eM_{\text{sat}}(1+\beta^2)} \tag{2}$$

is a prefactor determined by M_{sat}, the spin polarization P of the current, the electron charge e, and the Bohr magneton μ_{B}.

It has been shown that current-induced spin-orbit torques (SOT), typically generated at the same interfaces that induce DMI, can be a more efficient way to drive skyrmions. However, SOT-driven skyrmion motion is generally more complex than STT-driven motion because these torques also work in the out-of-plane direction and consequently change the (dynamic) equilibrium skyrmion size at large driving currents. Moreover, also the skyrmion Hall angle depends on the size of the driving current. These effects are intrinsic to the SOT-driven skyrmion motion, and are unrelated to the

interplay between the skyrmion breathing mode and the skyrmion velocity, which is the focus of this study. In order to avoid unnecessarily complicating the results, we therefore only consider Zhang-Li spin transfer torques as a skyrmion driving mechanism.

We simulate infinitely extended geometries by restricting the computation to a window centered around and moving with the magnetic structure under study while compensating the magnetic charges at the edges of the window when necessary [24]. As we consider infinitely thin films magnetized in the out-of-plane direction, the magnetostatic field can be accounted for by including it as an extra term in the anisotropy field to arrive at an effective anisotropy constant

$$K_{\text{eff}} = K_u - \frac{\mu_0}{2} {M_{\text{sat}}}^2, \tag{3}$$

allowing us to avoid the time-consuming calculation of the magnetostatic field in the simulations [25].

Moreover, a characteristic length $\delta = \sqrt{A_{\text{ex}}/K_{\text{eff}}}$ and a critical DMI strength $D_c = 4\sqrt{A_{\text{ex}} K_{\text{eff}}}/\pi$ can be defined [26], with the latter corresponding to the DMI strength at which the chiral domain wall energy becomes negative. In the following section, we will prove that the skyrmion size, when rescaled with δ, only depends on the parameter D/D_c.

2.2. Universal skyrmion size and breathing mode frequency

In order to extract the skyrmion diameter d from micromagnetic simulations where we have easy access to the average out-of-plane magnetization component m_z, we calculate d as

$$d = \sqrt{\frac{2S\,|m_z \pm 1|}{\pi}}, \tag{4}$$

with S the total area of the simulation window, and the plus (minus) sign corresponds to a positive (negative) out-of-plane skyrmion core magnetization in a background consisting of a negative (positive) out-of-plane magnetization. In order to investigate the skyrmion size, we let it relax to its equilibrium size by minimizing the energy towards its local minimum using a steepest descent method [27]. We performed this numerical experiment for 5 different sets of material parameters K_{eff}, A_{ex}, M_{sat}, detailed in Table 1.

As can be seen in Fig. 1, upon rescaling with δ, all diameters indeed coincide on one single universal curve which only depends on D/D_c. As the skyrmion size diverges for $D = D_c$, and finite-size effects of the simulation window started to manifest themselves, we do not show results for $D > 0.98 D_c$. For small values of $D < 0.65 D_c$, skyrmions are stable in the continuum limit up to infinitely small sizes. However, due to the finite size of the simulation cells, the skyrmions lose their stability in simulations nonetheless. In practice, this could be circumvented by considering smaller cell sizes. However, at these length scales the micromagnetic framework, which is a continuum approximation, is not longer physical, and we therefore do not consider these values either.

Parameter	A_{ex} (pJ/m)	K_{eff} (kJ/m^2)	M_{sat} (kA/m)	δ (nm)	D_c (mJ/m^2)	f_0 (GHz)
Set 1	16	510	580	5.60	3.64	7.84
Set 2	14	510	580	5.24	3.40	7.84
Set 3	16	400	580	6.32	3.22	6.15
Set 4	16	510	800	5.60	3.64	5.69
Set 5	14	400	800	5.92	3.01	4.46

Table 1. Material parameter sets used to illustrate the universality of the skyrmion diameter and breathing mode frequency, together with their respecive values for δ, D_c and f_0.

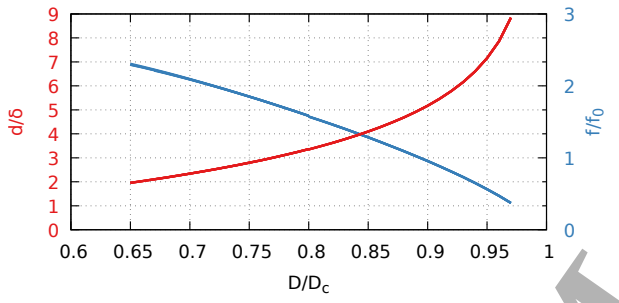

Figure 1. Universal curves (coinciding for all sets of material parameters) for the skyrmion diameter d (red curve, left axis), and breathing mode frequency f (blue curve, right axis) as function of D/D_c, rescaled with δ and f_0, respectively.

The aim of this paper is to investigate the skyrmion motion as it couples to the excitation of an internal mode. The best candidate is the skyrmion breathing mode, which is a dynamical mode defined by an oscillation of the skyrmion size around its equilibrium value [28, 29, 30]. In order to study this mode, we initialize the simulation from the relaxed skyrmion state, and excite it with a magnetic field pulse in the same out-of-plane direction as the skyrmion core magnetization to enlarge the skyrmion. After the pulse, the skyrmion size oscillations are simulated while they damp out towards the equilibrium size, and we determine the frequency of the breathing mode from at least 10 oscillations. We repeated these simulations for all sets of material parameters given in Table 1, and additionally verified that the extracted breathing mode frequency was independent of the field strength of the pulse and of the damping constant α. The amplitude of the excitation, however, depends strongly on the damping, and decreases at higher damping. The obtained results are shown in Fig. 1, and coincide when rescaled with $f_0 = \gamma K_{\mathrm{eff}}/\pi M_{\mathrm{sat}}$, corresponding to the precession frequency of a magnetic moment around the anisotropy axis. This implies that the obtained equilibrium size and breathing mode frequency can be rescaled to any set of material parameters.

2.3. Spin-transfer-torque induced skyrmion mobility

Before turning to the investigation of skyrmion motion through a notched nanotrack, we briefly review the skyrmion mobility through nanotracks in the absence of notches. A skyrmion can be driven either by a spin-transfer torque or spin-orbit torque [6]. As already mentioned, we only consider spin-transfer torques in our simulations. In any case, the skyrmion will generally move under an angle (called the skyrmion Hall angle) with respect to the current flow [6, 13, 31], so the skyrmion artificially needs to be guided along the desired track using one of the following methods. One method is to surround the nanotrack by a non-magnetic material [5], which generates a repulsing edge potential that forces the skyrmion to remain on its track [32]. Note, however, that this potential barrier can be overcome at large current densities, resulting in a collision between the skyrmion and the edge, and the subsequent annihilation of the skyrmion. A second option which suffers less from this disadvantage is to define the track by variations in the anisotropy constant between the nanotrack and its surroundings [33]. This can be achieved either by irradiating the track, so K_u lowers [34], or by placing a higher K_u material along the nanotrack edges [35]. In the region with higher K_u, the critical DMI constant D_c is higher, making it energetically favorable for the skyrmion to remain in the low K_u region, i.e. on the track. In our simulations, we will use a similar way to define the nanotracks by using a smaller DMI constant D_{edge} along the nanotrack edges, as suggested in Ref. [36]. Changing the DMI strength locally can be achieved by altering the thickness of the ferromagnetic layer, or more realistically, by using lithographic techniques to (partially) change or remove the DMI inducing nonmagnetic layer on top of the ferromagnet.

The skyrmion velocity $\mathbf{v}_{||}$, in the direction parallel to the current flow $\mathbf{v}_s = -b\mathbf{j}$, is given by Eq. (5), based on the Thiele equation [37, 38, 39]:

$$\mathbf{v}_{||} = \frac{\alpha\beta\left(\frac{\mathcal{D}}{\mathcal{G}}\right)^2 + 1}{\alpha^2\left(\frac{\mathcal{D}}{\mathcal{G}}\right)^2 + 1}\mathbf{v}_s. \tag{5}$$

In this equation, $\mathcal{G} = 4\pi Q$, where $Q = 1$ is the skyrmion number, and $\mathcal{D}$ is the dissipation tensor element [38], accounting for the skyrmion profile. As confirmed by Eq. (5), when $\alpha = \beta$, then $\mathbf{v}_{||} = \mathbf{v}_s$ and the skyrmion moves in the same direction as the electron flow [40, 41]. This could already be inferred from the LLG-equation, as its solution (given by Eq. (1)) is identical to the solution in the absence of a current while moving at a velocity $\mathbf{v} = -b\mathbf{j}$ when α and β are identical.

The focus of this paper lies on the interesting features displayed by the forward skyrmion motion along a nanotrack as it couples to periodically placed notches. To avoid an unnecessary elaboration on the details of the driving mechanism, we will therefore restrict ourselves to a spin-transfer-torque driven skyrmion in which α and β are equal. In most materials, this is not the case, and there the skyrmion will also display a sideways motion which will have to be abated by e.g. adapting the geometry of the notches or by using a system consisting of antiferromagnetically coupled layers in which the skyrmions show only forward motion[42]. We conclude this section by repeating that the skyrmion,

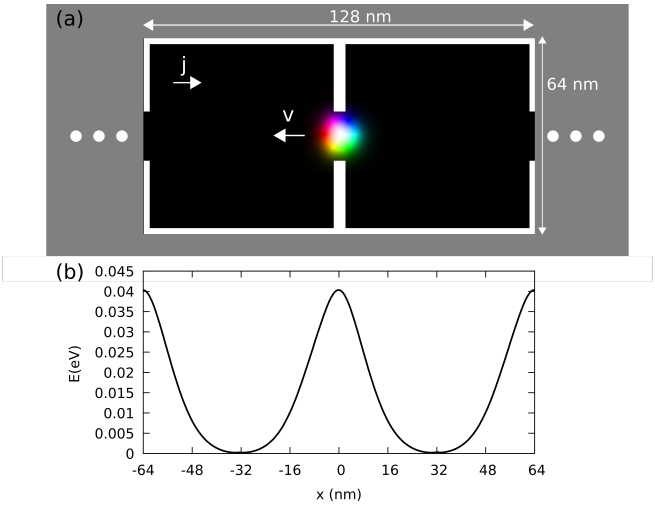

Figure 2. (a) Schematic of the system under study, consisting of an infinitely long nanotrack with periodically placed notches. The track edges and the notches are shown as white regions with a scaled down D_{edge}/D_c, compared to the D_{track}/D_c used in the nanotrack depicted as a black background (corresponding with a negative out-of-plane magnetization which contains a skyrmion. (b) Energy landscape as function of skyrmion position.

size, breathing mode frequency and velocity display universal behavior, and therefore, we will use only the first set of parameters from Table 1 in our simulations, without a loss of generality.

3. Results and Discussion

3.1. Skyrmion mobility in notched nanotracks

Skyrmions are insensitive to weak disorder [41] and move around geometric notches [5]. We will add notches the same way as we defined the edges of the nanotrack, i.e. by scaling-down the DMI constant D_{edge}. The system under study is shown in Fig. 2, and consists of a $128 \times 64 \times 0.4\,\text{nm}^3$ large simulation window, subdivided in finite difference cells of $0.5 \times 0.5 \times 0.4\,\text{nm}^3$. The skyrmion is initialized in the center, in between two 4 nm wide notches, laterally spaced 16 nm apart‡.

Both the notches and the nanowire edge have $D_{\text{edge}} = 0\,\text{J/m}^2$ and are represented by a white color in Fig. 2, while the track has $D_{\text{track}} = 0.75 D_c$. As the skyrmion travels to the left, the simulation window follows the skyrmion through the geometry in which the notches are repeated every 64 nm, and give rise to energy barriers with a height of about 40 meV.

‡ In our case the equilibrium skyrmion diameter is about 15 nm. In most experimental systems under study today, the DMI constant is such that the observed skyrmions are larger than the ones used in our example. Therefore, the entire system geometry will have to be scaled accordingly when trying to experimentally verify our findings, and the smallest features will be significantly larger than the 4 nm used here, facilitating the experimental realization of this study.

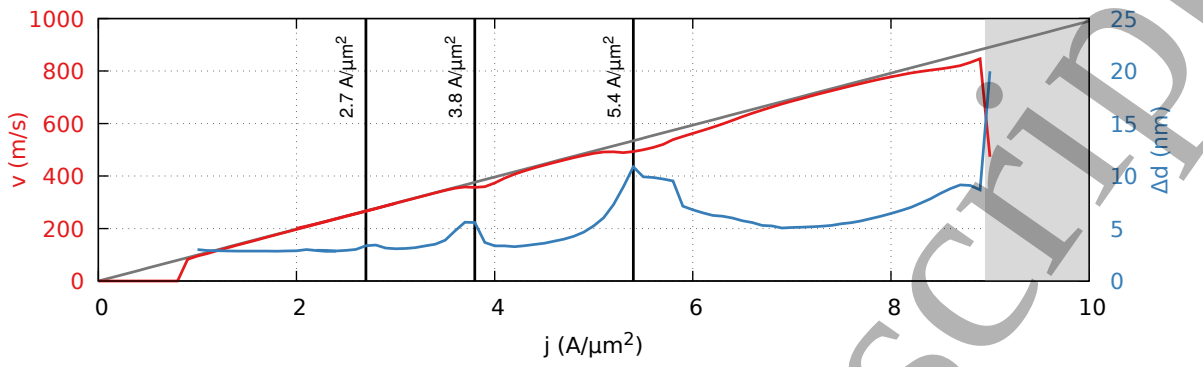

Figure 3. Skyrmion velocity v (red curve) and size fluctuations Δd (blue curve) for a skyrmion driven by a current density j through a notched nanotrack. The current is initialized at $2\,\mathrm{A}/\mu\mathrm{m}^2$ and ramped up/down from there. The gray line shows the velocity in the absence of notches and the black labels show the position of the resonances in Δd.

We now take a look at Fig. 3 which shows the results for the STT-current driven skyrmion motion in a periodically notched nanotrack. In this simulation, the current density was initialized at $j = 2\,\mathrm{A}/\mu\mathrm{m}^2$, and was then ramped up every 10 ns in steps of $0.1\,\mathrm{A}/\mu\mathrm{m}^2$ until the skyrmion annihilated at $j \approx 9\,\mathrm{A}/\mu\mathrm{m}^2$. Subsequently, the simulation was repeated, but the current was ramped down to find the dynamic pinning threshold at $j \approx 1\,\mathrm{A}/\mu\mathrm{m}^2$.

As compared to the linear relation between current density and velocity found in a nanotrack without notches (gray line), the mobility now displays two additional features. Firstly, at low current densities, the skyrmion is unable to pass through the notches and gets pinned. Secondly, the velocity displays plateaus of almost constant velocity. These two features explain our choice for $j = 2\,\mathrm{A}/\mu\mathrm{m}^2$ to start the simulations from, because it is both higher than the depinning threshold, and smaller than the currents at which the mobility curve starts to display velocity plateaus.

The mechanism behind the plateaus can be understood when looking at the velocities at which they occur, i.e. 360 m/s and 490 m/s. At these velocities, it takes the skyrmion $t_1 = 177\,\mathrm{ps}$ and $t_2 = 130\,\mathrm{ps}$, respectively, to cover the 64 nm distance between two notches. Using the results from Fig. 1, we determine the breathing mode period to be $(1.85 f_0)^{-1} = 69\,\mathrm{ps}$. Although there is only a very rough agreement between $t_1/3 = 59\,\mathrm{ps}$, $t_2/2 = 65\,\mathrm{ps}$ and this value, we postulate that the skyrmion breathing mode gets resonantly excited when the skyrmion velocity is such that the time interval between two notches equals a small multiple of the breathing mode period. The very rough agreement can be understood because, the skyrmion is confined by the track edges and the notches, causing the period to decrease [29] in comparison with its value determind for an infinite film in Fig. 1.

The excitation of the breathing mode is further evidenced by the blue curve in Fig. 3, which shows Δd, the difference between the minimum and maximum diameter

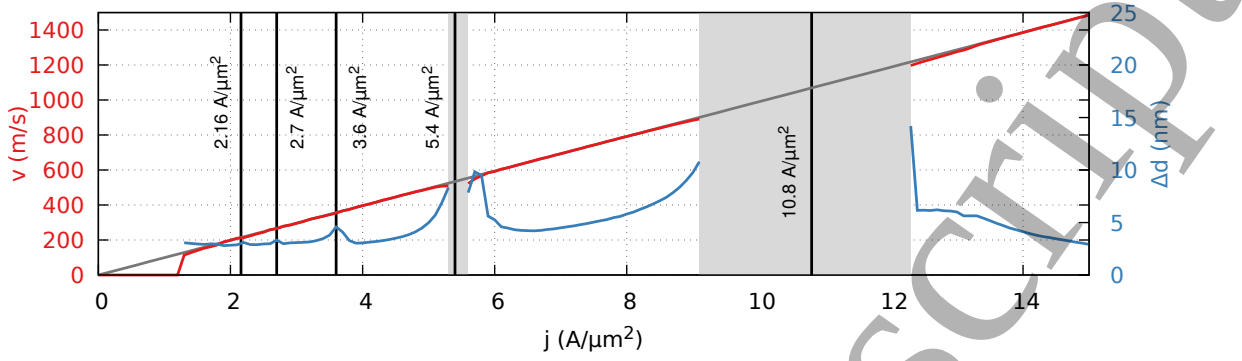

Figure 4. Skyrmion velocity v (red curve) and size fluctuations Δd (blue curve) for a skyrmion driven by a current density j through a notched nanotrack. The current is applied instantaneously to a skyrmion at rest. The gray line shows the velocity in the absence of notches and the black labels show the position of the resonances in Δd.

attained by the skyrmion during its motion. Indeed, Δd displays clear maxima at the current densities of 3.8 and 5.4 $\mathrm{A}/\mu\mathrm{m}^2$ where we found the velocity plateaus. There also is a small peak visible at 2.7 $\mathrm{A}/\mu\mathrm{m}^2$, which corresponds to 4 breathing mode periods. This figure also explains why the skyrmion annihilates at high current densities: the skyrmion is excited so strongly that the minimal skyrmion size during its oscillation is too small for the cell size to support the stability of the skyrmion (indicated by the gray areas in Fig. 3).

We now repeat this study, but instead of ramping the current up (or down), for each current density, the skyrmion is re-initialized in its equilibrium state at rest before applying the current for 10 ns. The results shown in Fig. 4 display two marked differences as compared to the case in which the current was ramped. Here, for instance, the resonances in the skyrmion size are stronger: the skyrmion already annihilates at $j = 5.4\,\mathrm{A}/\mu\mathrm{m}^2$, and there is a very slight peak visible at 2.16 $\mathrm{A}/\mu\mathrm{m}^2$, corresponding to 5 periods of the breathing mode. From these values we deduce that the one period current density must be found at approximately $j = 10.8\,\mathrm{A}/\mu\mathrm{m}^2$. Strikingly, in contrast to the ramped current case, the skyrmion velocity displays no plateaus.

Both differences lead us to the conclusions that probably, if we would have ramped the current more slowly, the results of Fig. 3 would converge to the results presented in Fig. 4 and, more importantly, that the velocity plateaus visible in the ramped case are a dynamical effect in which the skyrmion robustly keeps moving at its resonant velocity for some time after it is perturbed. This is further supported by the fact that the peaks in Δd are slightly shifted towards larger current densities when ramping the current up, e.g. 3.6 $\mathrm{A}/\mu\mathrm{m}^2$ in Fig. 4 vs. 3.8 $\mathrm{A}/\mu\mathrm{m}^2$ in Fig. 3.

Let's now take a closer look at the coupling between the skyrmion motion and its breathing mode at the resonant current densities. Figure 5 shows the skyrmion size as function of its position at the current densities indicated by black lines in Fig. 4, with the exception of $j = 10.8\,\mathrm{A}/\mu\mathrm{m}^2$ and $j = 5.4\,\mathrm{A}/\mu\mathrm{m}^2$, where the skyrmion was unstable.

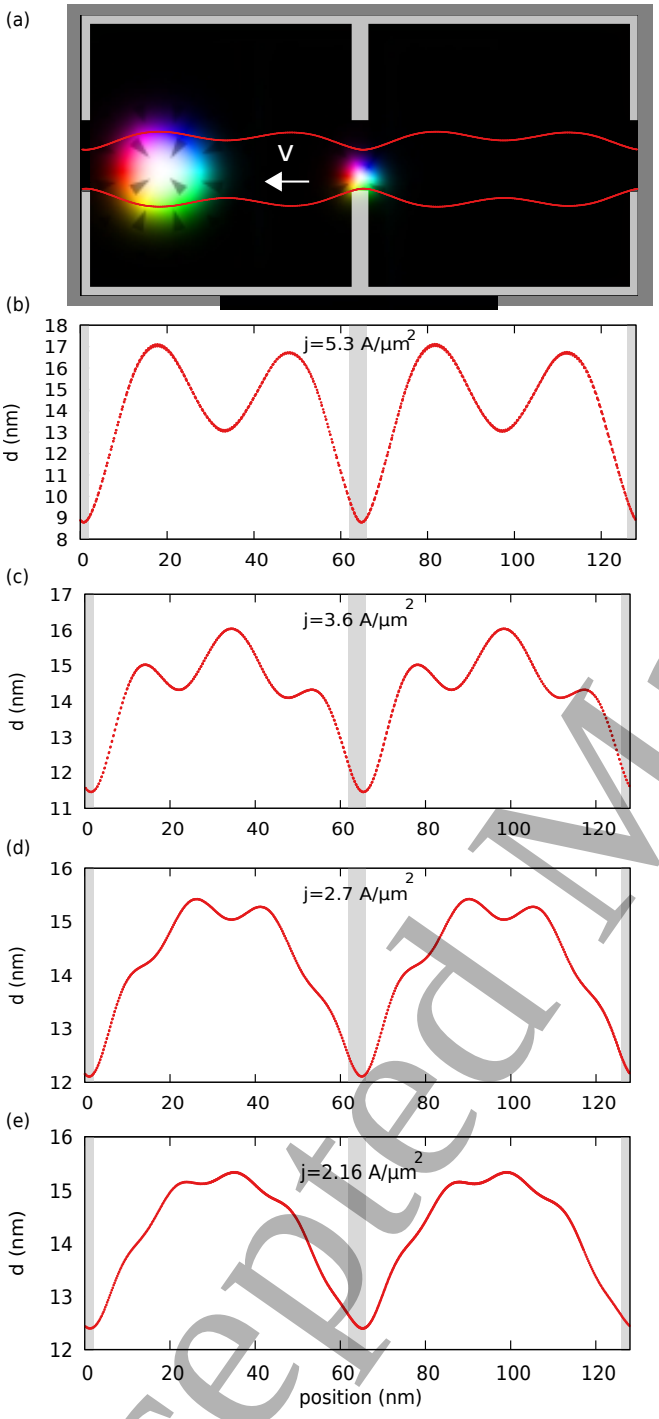

Figure 5. Skyrmion diameter (red lines) as function of position during its motion through the notched nanotrack at the resonances corresponding to 2 (a) and (b), 3 (c), 4 (d) and 5 (e) skyrmion breathing periods, in between two consecutive notches.

Instead of the latter, we show the skyrmion size at $j = 5.3\,\mathrm{A}/\mu\mathrm{m}^2$. As expected, the skyrmion diameter is minimal when it passes through the notches (represented by the gray areas) and the number of local maxima in the skyrmion size in between each notch confirms once again that the plotted velocities indeed correspond to 2 ($5.4\,\mathrm{A}/\mu\mathrm{m}^2$), 3

(3.6 A/μm^2), 4 (2.7 A/μm^2), and 5 (2.16 A/μm^2) periods of the breathing mode. Fig. 5 (a) depicts the outer skyrmion diameter as function of position and shows that the skyrmion is moving off center. Indeed, as soon as the skyrmion deviates slightly from the nanotrack center, the side closest to the track edge experiences more drag when moving through the notches and thus deviates further in this direction. In between these resonant current densities the skyrmion size oscillates still periodically, but at a lower amplitude, and the profile lies in between the two closest resonant profiles. The skyrmion motion for all current densities shown in Fig. 5, and for $j = 4.5\,\mathrm{A}/\mu\mathrm{m}^2$ (in between the 2 and 3 period resonances) are shown in the supplementary movies.

3.2. DMI strength and notch separation variations

To gain further insight in the interplay between the skyrmion motion and the confining potential of the notched nanotrack, we perform an additional set of simulations in which we vary D_{edge}/D_c from 0 to 0.70 with intermediate values at 0.15, 0.30, 0.45, 0.50 and 0.60 ($D_{\mathrm{track}} = 0.75D_c$). The results are depicted in Fig. 6 (a) which shows Δd as function of current density for all simulated values of D_{edge}. As expected, the excitation of the breathing modes, and hence Δd become larger for smaller values of D_{edge}. Notably, the skyrmion gets excited even when D_{edge} is only slightly smaller than D_{track}, and, except for the value closest to D_{track}, the excitation is so strong that the skyrmion loses its stability at the one period resonance. The peaks corresponding with two and three size oscillations per notch are clearly visible in all systems, and shift towards higher velocities for smaller D_{edge}. We extracted the breathing mode periods corresponding to these peaks, and show them as closed (2 oscillations) and open (3 oscillations) red dots in Fig. 6 (b). The blue horizontal line corresponds to the breathing mode period $(1.85f_0)^{-1} = 69\,\mathrm{ps}$ determined from Fig. 1. As expected, the agreement is best for D_{edge} close to D_{track}, where the skyrmion feels the lowest confinement. The observed trend can be understood because the breathing mode period decreases in stronger confining potentials, associated with small D_{edge} values.

In a next set of simulations, we varied the distance between two consecutive notches with $D_{\mathrm{edge}} = 0$ as 48 nm, 64 nm and 96 nm. The main effect was that the driving currents at which we observed resonances in Δd scaled linearly with this distance, but there were additional differences. We extracted the breathing mode period by averaging over all stable 2, 3, 4 and 5-period resonances and added them to Fig 6 as a green and purple dot for the 48 and 96 nm separated notches, respectively. Their position relative to the blue line (corresponding to an infinite film) and red dot (corresponding to the 64 nm notch distance), are again explained by the fact that the skyrmion feels a stronger confining potential in closely spaced notches. Furthermore, we observed that the smaller confinement for the larger distances is also reflected in overall larger Δd for larger distances.

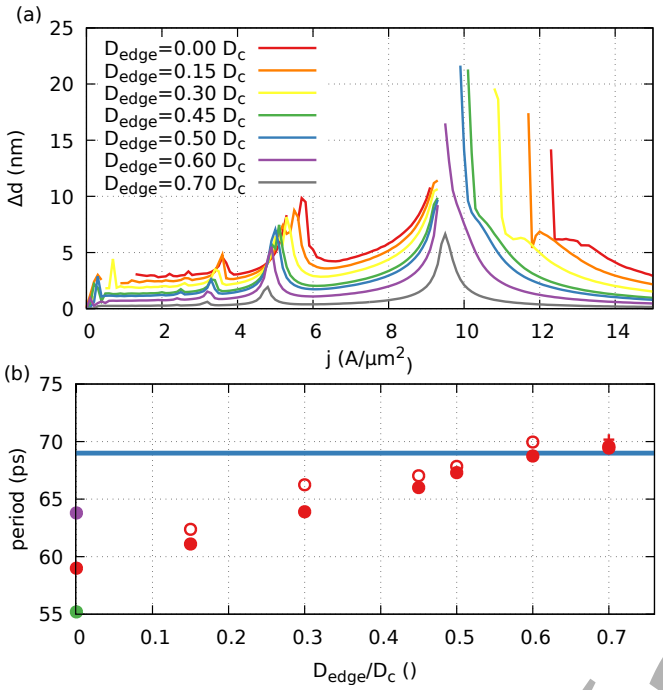

Figure 6. (a) Skyrmion size fluctuations Δd as function of current density j for several different D_{edge} values, while $D_{\text{track}} = 0.75 D_c$ in all simulations. (b) Skyrmion breathing mode period as function of D_{edge}. The blue lines shows the period in an infinite film, extracted from the data depicted in Fig. 1. The red open (closed) dots represent the periods extracted from the two (three) period oscillations in panel (a). The red plus (overlapping the dots at $D_{\text{edge}} = 0.7 D_c$) corresponds to the only stable one period oscillation (depicted by the gray line in (a)). The green and purple dots correspond to the average period extracted from simulations with a notch distance of 48 and 96 nm, respectively.

3.3. Domain wall mobility in notched nanotracks

In this section, we divert from the study of skyrmion mobility and compare our results to the motion of a domain wall through a periodically notched, in-plane magnetized nanotrack. The plateaus in the skyrmion velocity originated in the coupling between the forward motion of the skyrmion and the excitation of the skyrmion breathing mode. However, in contrast to skyrmions, domain walls are usually considered to be rigid objects whose behavior can be explained excellently without having to account for any internal dynamics [43].

We investigate the STT-current driven motion of a transverse domain wall through a notched permalloy nanotrack. As shown in Fig. 7, we simulate an infinitely long nanotrack with a width of 100 nm and a thickness of 10 nm. The moving simulation window, following the transverse domain wall, has a length of 800 nm, spans the full width and thickness of the track, and is subdivided in finite difference cells of $3.125 \times 3.125 \times 10\,\text{nm}^3$. Permalloy is a soft magnetic material with $M_{\text{sat}} = 860\,\text{kA/m}$, $A_{\text{ex}} = 13\,\text{pJ/m}$, spin polarization $P = 0.6$ and $\alpha = 0.01$, specifically designed to have no magnetostriction or anisotropy ($K_u = 0$). Furthermore, it has no DMI. The latter

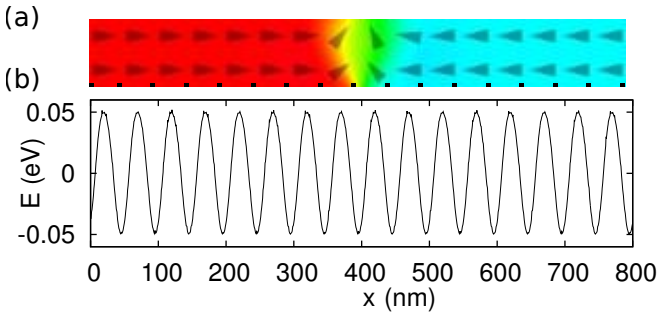

Figure 7. (a) transverse domain wall in the permalloy nanotrack. The arrows and colors represent the magnetization direction and the notches are depicted in black at the bottom of the nanotrack. (b) Potential energy landscape as function of position for the system shown in (a).

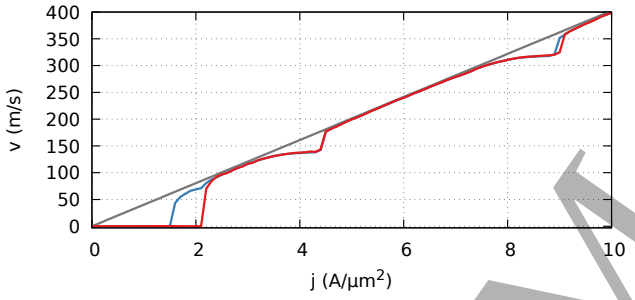

Figure 8. Transverse domain wall velocity in a permalloy nanotrack without (gray line) and with notches (red and blue line). The blue line results from a simulation in which the current was ramped down from $j = 10\,\mathrm{A}/\mu\mathrm{m}^2$ and the red line from a simulation in which the current was applied instantaneously to a domain wall at rest for each current density.

property prevents us to include notches with lower D_{edge} as in the skyrmion nanotrack. Instead, at one side of the track, we introduce regions of 2 by 2 finite difference cells, spaced 50 nm apart, with a scaled-down exchange coupling at their edges. In order for the notches to resemble realistic material defects, the exchange coupling is scaled down by 50% [44, 45].

The energy landscape U felt by the domain wall as function of its position was extracted from the simulations and is shown in Fig. 7, which shows that the notches give rise to sinusoidal potential landscape with potential wells of approximately 0.1 eV, in agreement with literature values for measured material defects [46].

To investigate the motion of the transverse domain wall, we perform similar simulations as for the skyrmion nanotrack. In an ideal nanotrack, in the absence of any disorder or notches, a STT-driven domain wall displays a linear relation between the current density and velocity [47, 48], as shown by the gray line in Fig. 8. If $\alpha \neq \beta$, the picture would be further complicated by the presence of an intrinsic depinning threshold or a Walker breakdown [48], but as these effects are well understood already, we restrict

ourselves again to the case with $\alpha = \beta$, so we can focus on the effects on the forward motion.

Analogously as in the simulations of skyrmion mobility, the current is applied in two ways. Firstly, before applying a certain current density j, the domain wall is initialized from its equilibrium position pinned to a notch. Then the current is switched on and the domain wall motion is simulated for 20 ns, which is more than sufficient for the motion to attain a steady state. Secondly, we start from the simulation at $j = 10\,\mathrm{A}/\mu\mathrm{m}^2$ and the current density is ramped down at a velocity of $5\,\mathrm{A}/\mu\mathrm{m}^2/\mu\mathrm{s}$. The former corresponds to the red curve in Fig. 8, while the latter corresponds to the blue curve. From approximately $j \approx 2\,\mathrm{A}/\mu\mathrm{m}^2$ onwards, the red and blue curve coincide, and show two velocity plateaus at approximately $v = 140\,\mathrm{m/s}$ and $v = 310\,\mathrm{m/s}$. However, these plateaus are unlike the plateaus observed in the skyrmion case in two ways. On the one hand, the first plateau does not correspond to the excitation of an internal mode of the domain wall, but instead the domain wall as a whole makes an oscillatory motion from one notch to the next. The second plateau does, however, correspond to the excitation of an internal mode. The domain wall motion at both of these resonant velocities, as well as at an intermediate velocity are shown in the supplementary movies. Secondly, the fact that the blue and red curve coincide proves that, unlike the skyrmion case, the domain wall gets into this resonance disregarding whether it was directly excited at the relevant current density, or whether it was slowly approached from a different current density. This means that this mechanism to stabilize the velocity might be better suited to domain wall based devices, than their skyrmion counterparts. Finally, at low current densities, an extrinsic depinning threshold is visible due to the pinning at the notches. The differences between the depinning current threshold displayed by the red and blue curve are discussed in detail in the next section.

3.4. Low current and bistable regimes

To understand the behavior at current densities below $3\,\mathrm{A}/\mu\mathrm{m}^2$ we take a closer look at the potential landscape the domain wall moves through. In the presence of a driving force, the sinusoidal landscape gets tilted and is typically called a washboard potential.

Generally speaking, there exist three different mobility regimes, corresponding to the size of the tilt of the potential. In the first regime, called the pinned regime, the driving force is too weak to sustain any motion. A domain wall at rest in a local energy minimum will stay at rest, and a moving domain wall will dissipate its energy and come to a stop. This regime is schematically depicted in panel (b) of Fig. 9 and corresponds to current densities below $1.5\,\mathrm{A}/\mu\mathrm{m}^2$ in panel (a).

In between the low and high driving force regimes, there is an intermediate regime, in which the motion can enter two possible states [49]. First, there is a locked state, in which the driving force does not suffice to push the domain wall out of the potential well. In this case, the wall will come to a rest in an equilibrium position where the

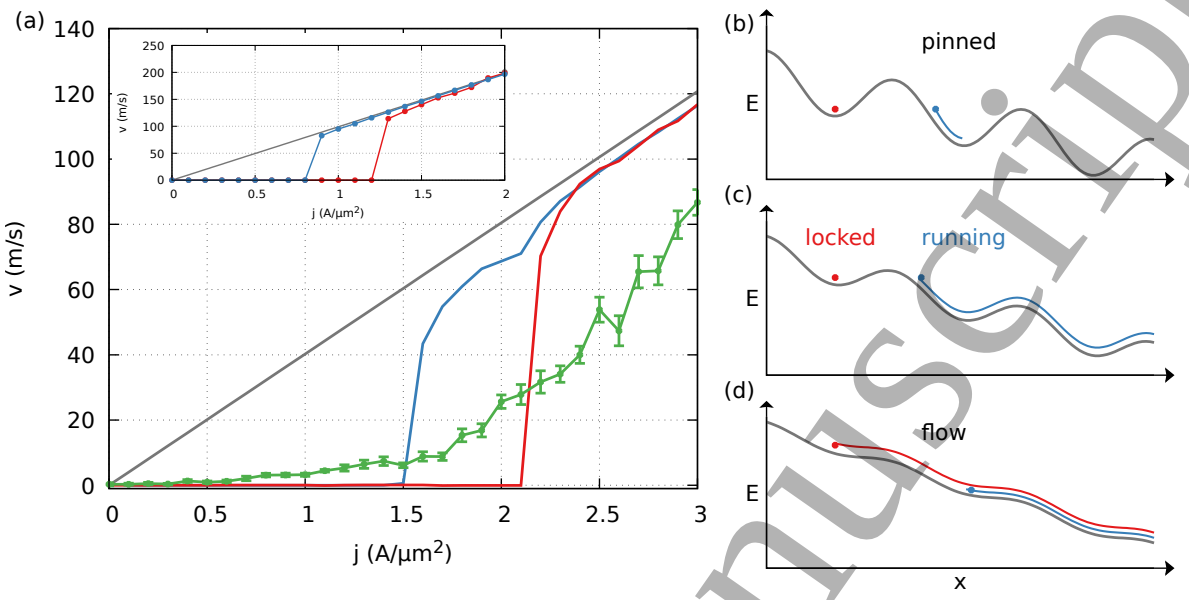

Figure 9. (a) Domain wall velocity in a notched nanotrack as function of current density. The red and blue lines correspond to a current that was ramped down from a high value and which was applied instantaneously to a domain wall at rest, respectively, while the gray curve shows the mobility in the absence of notches. The green curve shows the mobility at a temperature of 300 K, displaying creep behavior. The inset shows the same data at zero temperature for skyrmion mobility. Panels (b), (c), and (d), schematically show the relation between the motion and the energy landscape in the pinned, locked (red dot) and running (blue dot), and flow state, as indicated by the labels. The red and blue colors were chosen to correspond to the mobility displayed in panel (a).

driving force and the force due to the potential well are balanced. Secondly, a running solution exists, in which the wall has enough speed to overcome the barriers in between the potential wells and keeps moving along the nanotrack. In this solution, the velocity will oscillate depending on the position in the periodic energy landscape but will be nonzero on average. The threshold current density between these two regimes depends on the initial velocity and position of the domain wall. For instance, the red mobility curve in Fig. 9 (a) corresponds to a domain wall initialized at rest, while the blue curve corresponds to a domain wall which was initialized in motion, and consequently remained in motion down to much lower current densities. The locked and running state are schematically depicted by the red and blue dot in panel (c), respectively.

Finally, in the flow regime, the driving force is sufficiently strong so the tilt in the potential landscape causes the local minima to disappear, and the domain wall will always move forward. In Fig. 9, where this regime is schematically shown in panel (d), this corresponds to the region where the red and blue curve coincide in panel (a).

At nonzero temperatures, thermal fluctuations can help the domain wall to

overcome the energy barriers due to the notches, drastically affecting its mobility. To investigate this regime, we perform an additional set of simulations at a temperature of 300 K. In the micromagnetic framework, temperature is added as a stochastic effective field term to the LLG-equation [50, 51], which we then solve using an adaptive timestepping method detailed in Ref. [52]. The green line in Fig. 9 shows the average velocities and their uncertainties extracted from 10 such simulations, in which each current density was applied for 100 ns. Instead of the pinned regime found at 0 K, we now see a creep regime in which the domain wall makes thermal jumps from one local energy minimum to the next. In a previous study we investigated the motion of a domain wall in the creep regime by deriving an equation which approximates the domain wall as a rigid object and describes its motion through nanotracks with an arbitrary energy landscape at finite temperatures [53, 54]. For a randomly disordered nanotrack, we found a linear velocity-current creep scaling law at low current densities. We solved the equation again for a periodically notched nanotrack and again find a linear relation between the velocity and current.

In the intermediate current regime, a third possible state is found in which the domain wall switches between the locked and running state, and is therefore called the bistable state [49]. In this state, as shown schematically in Fig. 10, the domain wall enters the running state and moves forward until, at a random point in time, thermal fluctuations cause it to lose too much energy and become trapped. At a still later time, the thermal fluctuations can then cause the wall to gain enough energy to overcome the energy barrier and enter the running state again, until the process repeats itself.

Note that it is not trivial that the velocity shown in Fig. 9 at 300 K seems lower than the velocity found at 0 K. The reason for this counterintuitive behavior lies in the fact that the red curve corresponds to the velocity of the domain wall when the current density is instantaneously turned on. If the current density is slowly ramped up, the domain wall, which in fact is not a completely rigid object [55], can adapt its profile to the new situation and the onset of the flow regime shifts to much higher current densities.

We now turn our attention back to skyrmion mobility. The low current regimes of Fig. 3 and Fig. 4 are repeated in the inset of Fig. 9, as a blue and red curve corresponding to the running and locked regime, respectively. This figure shows that the skyrmion motion through a notched nanotrack at low current densities is qualitatively the same as domain wall motion and also consists of a pinned, locked, running, and flow state.

Although a full study of the thermally assisted skyrmion mobility lies beyond the scope of this article, we like to point out that the dynamics displayed in the bistable regime are very similar to the operating principle of a skyrmion reshuffler based on the combination of a driving current and thermal diffusion [56]. A reshuffler is a key component in probabilistic computing as it uncorrelates two signals while preserving the ratio of '1's and '0's in a bit sequence. This is important because this ratio determines the outcome of the actual computation. The reshuffler presented in Ref. [56] consists of

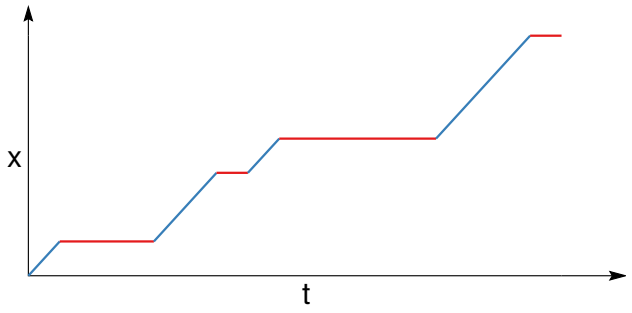

Figure 10. Schematic representation of the stochastic motion in the bistable regime, switching between the running (blue lines) and locked (red lines) state.

two distinct tracks (one for each bit) through which the skyrmions are driven by a DC current. Similar to the time necessary for a skyrmion to run through a nanotrack with a periodically modulated potential, once the skyrmions enter the reshuffle chamber, the moment at which they escape again is stochastically determined by the combination of the driving current and thermal diffusion.

4. Conclusions and outlook

In this paper we investigated the motion of skyrmions and domain walls through nanotracks with periodically placed notches, consisting of areas with reduced DMI constant. Alternatively, we could have divided the track over its full width into a periodic sequence of regions with different DMI values. Instead of passing through notches, the skyrmions would then have to move over these regions. In our study, the notches dynamically excite the breathing mode when the skyrmion velocity is such that the time necessary to move between two consecutive notches coincides with a small multiple of the breathing mode period. This manifests itself as a peak in the diameter oscillations during the skyrmion motion. Moreover, this coupling between the mobility and the nanotrack geometry makes the skyrmion velocity robust against small perturbations. More specifically, we showed that the skyrmion velocity remains constant when ramping the driving current density. For most notch parameters used in our study, the breathing mode excitation was so strong that the skyrmion could collapse when driven at its resonant velocity. This can however be mitigated as we have shown that notches with a very weak potential are already able to excite the skyrmion, and do not cause it to collapse.

We provided an explanation based on the skyrmion breathing mode why the resonances are found at certain velocities, which can be used to tune the notch parameters, e.g., their separation distance, to bring the resonant velocity to any desired value. This might offer a strategy to stabilize the velocity in racetrack memory devices against unwanted external perturbations like Oersted fields, often encountered in technological applications.

We focused on spin-transfer-torque driven motion, but we checked that the coupling between the skyrmion breathing mode and its velocity remains visible in the case of spin-orbit-torques driven motion. Therefore, the results can in principle also be extended to SOT-driven skyrmion motion, albeit at the cost of additional complexity due to the current-dependence of the skyrmion size and Hall-angle.

Despite the fact that domain walls are much more rigid objects, we were able to extend our results to domain wall motion as well. As compared to the skyrmion mobility, the domain wall velocity displays large plateaus at which the domain wall oscillates, rendering this system even more robust against driving force variations.

In the last part of this paper, we discussed the motion at low driving forces, and considered the effect of nonzero temperatures to show the similarities between the bistable mobility regime and the dynamics behind the skyrmion reshuffler device. This illustrates that the dynamics studied in this paper are useful for racetrack-like memory devices, but also lie at the foundation of state-of-the-art probabilistic skyrmion logic devices.

We conclude that the mobility of nanomagnetic structures through notched nanotracks show very rich dynamics that are not only interesting from a fundamental point of view, but also show potential in different spintronic applications. Following the recent numerical [52] and experimental [56] advances in thermally active systems, we remark that further studies directed at thermally assisted motion will be necessary to realize the full potential of these applications.

Acknowledgment

This work is supported by Fonds Wetenschappelijk Onderzoek (FWO-Vlaanderen) through Project No. G098917N. J.L acknowledges his postdoctoral fellowships by the Ghent University special research fund (BOF) and FWO-Vlaanderen. The authors gratefully acknowledge the support of NVIDIA Corporation through donation of Titan Xp and Titan V GPU cards used for this research.

[1] Allwood D A, Xiong G, Faulkner C C, Atkinson D, Petit D and Cowburn R P 2005 *Science* **309** 16881692
[2] Zhang X, Ezawa M and Zhou Y 2015 *Sci. Rep.* **5** 9400
[3] Parkin S P, Hayashi M and Thomas L 2008 *Science* **320** 190–194
[4] Parkin S and Yang S H 2015 *Nat. Nanotechnol.* **10** 195–198
[5] Fert A, Cros V and Sampaio J 2013 *Nat. Nanotechnol.* **8** 152–156 ISSN 1748-3387
[6] Tomasello R, Martinez E, Zivieri R, Torres L, Carpentieri M and Finocchio G 2014 *Sci. Rep.* **4** 6784
[7] Dzyaloshinsky I 1958 *J. Phys. Chem. Solids* **4** 241–255
[8] Dzyaloshinskii I E 1964 *Sov. Phys. JETP* **19** 960
[9] Moriya T 1960 *Phys. Rev.* **120** 91–98
[10] Crépieux A and Lacroix C 1998 *J. Magn. Magn. Mater.* **182** 341–349
[11] Romming N, Hanneken C, Menzel M, Bickel J E, Wolter B, von Bergmann K, Kubetzka A and Wiesendanger R 2013 *Science (New York, N.Y.)* **341** 636–639
[12] Woo S, Litzius K, Krüger B, Im M Y, Caretta L, Richter K, Mann M, Krone A, Reeve R M,

Weigand M, Agrawal P, Lemesh I, Mawass M A, Fischer P, Klaui M and Beach G S D 2016 *Nat. Mater.* **15** 501 ISSN 1476-4660
[13] Litzius K, Lemesh I, Krüger B, Bassirian P, Caretta L, Richter K, Büttner F, Sato K, Tretiakov O A, Frster J, Reeve R M, Weigand M, Bykova I, Stoll H, Schtz G, Beach G S D and Kläui M 2016 *Nat. Phys.* **13** 170–175
[14] Woo S, Song K M, Zhang X, Ezawa M, Zhou Y, Liu X, Weigand M, Finizio S, Raabe J, Park M C, Lee K Y, Choi J W, Min B C, Koo H C and Chang J 2018 *Nat. Electron.* **1** 288–296
[15] Yuan H and Wang X 2015 *Phys. Rev. B* **92** 054419
[16] Nakatani Y, Thiaville A and Miltat J 2003 *Nat. Mater.* **2** 054419
[17] Fook H T, Gan W L and Lew W S 2016 *Sci. Rep.* **6**
[18] Stosic D, Ludermir T B and Milošević M V 2017 *Phys. Rev. B* **96**(21) 214403
[19] Reichhardt C and Reichhardt C J O 2015 *Phys. Rev. B* **92** 224432
[20] Vansteenkiste A, Leliaert J, Dvornik M, Helsen M, Garcia-Sanchez F and Van Waeyenberge B 2014 *AIP Adv.* **4** 107133
[21] Leliaert J, Dvornik M, Mulkers J, De Clercq J, Milošević M V and Van Waeyenberge B 2018 *J. Phys. D: Appl. Phys.* **51** 123002
[22] Landau L D and Lifshitz E M 1935 *Phys. Z. Sowietunion* **8** 153
[23] Zhang S and Li Z 2004 *Phys. Rev. Lett.* **93** 127204
[24] Leliaert J, Van de Wiele B, Vansteenkiste A, Laurson L, Durin G, Dupré L and Van Waeyenberge B 2014 *J. Appl. Phys.* **115** 233903
[25] Coey J M D 2010 *Magnetism and Magnetic Materials* (Cambridge University Press) ISBN 9780511845000
[26] Rohart S and Thiaville A 2013 *Phys. Rev. B* **88** 184422
[27] Exl L, Bance S, Reichel F, Schrefl T, Stimming H P and Mauser N J 2014 *J. Appl. Phys.* **115** 17D118
[28] Büttner F, Moutafis C, Schneider M, Krüger B, Günther C M, Geilhufe J, Schmising C v K, Mohanty J, Pfau B, Schaffert S, Bisig A, Foerster M, Schulz T, Vaz C A F, Franken J H, Swagten H J M, Kläui M and Eisebitt S 2015 *Nat. Phys.* **11** 225–228
[29] Kim J V, Garcia-Sanchez F, Sampaio J, Moreau-Luchaire C, Cros V and Fert A 2014 *Phys. Rev. B* **90**(6) 064410
[30] Mochizuki M 2012 *Physical Review Letters* **108**
[31] Jiang W, Zhang X, Yu G, Zhang W, Wang X, Jungfleisch M B, Pearson J E, Cheng X, Heinonen O, Wang K L, Zhou Y, Hoffmann A and te Velthuis S G E 2016 *Nature Physics* **13** 162–169
[32] Iwasaki J, Mochizuki M and Nagaosa N 2013 *Nat. Nanotechnol.* **8** 742
[33] Song C, Jin C, Wang J, Xia H, Wang J and Liu Q 2017 *Applied Physics Letters* **111** 192413
[34] Fook H T, Gan W L, Purnama I and Lew W S 2015 *IEEE Trans. Magn.* **51** 1–4
[35] Lai P, Zhao G P, Tang H, Ran N, Wu S Q, Xia J, Zhang X and Zhou Y 2017 *Sci. Rep.* **7** 45330
[36] Mulkers J, Van Waeyenberge B and Milošević M V 2017 *Phys. Rev. B* **95** 144401
[37] Thiele A A 1973 *Phys. Rev. Lett.* **30** 230–233
[38] Iwasaki J, Mochizuki M and Nagaosa N 2013 *Nat. Commun.* **4** 1463
[39] He J, Li Z and Zhang S 2006 *Phys. Rev. B* **73** 184408
[40] Schütte C, Iwasaki J, Rosch A and Nagaosa N 2014 *Phys. Rev. B* **90** 174434
[41] Müller J and Rosch A 2015 *Phys. Rev. B* **91** 054410
[42] Zhang X, Zhou Y and Ezawa M 2016 *Nature Communications* **7** 10293
[43] Thiaville A, Nakatani Y, Miltat J and Suzuki Y 2005 *Europhys. Lett.* **69** 990–996
[44] Leliaert J, Van de Wiele B, Vansteenkiste A, Laurson L, Durin G, Dupré L and Van Waeyenberge B 2014 *J. Appl. Phys.* **115** 17D102
[45] Paixão E L M, Toscano D, Gomes J C S, Monteiro M G, Sato F, Leonel S A and Coura P Z 2018 *J. Magn. Magn. Mater.* **451** 639–646
[46] Burgess J A J, Fraser A E, Sani F F, Vick D, Hauer B D, Davis J P and Freeman M R 2013 *Science* **339** 1051–1054

[47] Leliaert J, Van de Wiele B, Vansteenkiste A, Laurson L, Durin G, Dupré L and Van Waeyenberge B 2014 *Phys. Rev. B* **89** 064419
[48] Boulle O, Malinowski G and Kläui M 2011 *Mater. Sci. Eng., R* **72** 159–187 ISSN 0927-796X
[49] Vollmer H D and Risken H 1979 *Z. Phys. B: Condens. Matter* **34** 313–322
[50] Lyberatos A, Berkov D and Chantrell R W 1993 *J. Phys.: Condens. Matter* **5** 8911
[51] Brown W F 1963 *Phys. Rev.* **130**(5) 1677–1686
[52] Leliaert J, Mulkers J, De Clercq J, Coene A, Dvornik M and Van Waeyenberge B 2017 *AIP Adv.* **7** 125010
[53] Leliaert J, Van de Wiele B, Vandermeulen J, Coene A, Vansteenkiste A, Laurson L, Durin G, Van Waeyenberge B and Dupré L 2015 *Appl. Phys. Lett.* **106** 202401
[54] Leliaert J, Van de Wiele B, Vansteenkiste A, Laurson L, Durin G, Dupré L and Van Waeyenberge B 2016 *Sci. Rep.* **6** 20472
[55] Hayward T J and Omari K A 2017 *J. Phys. D: Appl. Phys.* **50** 084006
[56] Zázvorka J, Jakobs F, Heinze D, Keil N, Kromin S, Jaiswal S, Litzius K, Jakob G, Virnau P, Pinna D, Everschor-Sitte K, Dongesb A, Nowak U and Kläui M 2018 *arXiv preprint arXiv:1805.05924*